J Solid State Electrochem (2009) 13:1403–1409
DOI 10.1007/s10008-008-0705-1

ORIGINAL PAPER

Enhanced electrochemical activity for ethanol oxidation on the carbon-supported Pt_3Te nanocatalysts by addition of Ru

Meihua Huang · Lirong Li · Yonglang Guo

Received: 1 September 2008 / Revised: 5 October 2008 / Accepted: 7 October 2008 / Published online: 21 October 2008

Abstract Ternary Pt–Te–Ru catalysts with different atomic ratios were synthesized by reducing the precursor with formic acid. The physical and electrochemical characterization of the $Pt_3TeRu_{0.25}$/C catalyst was performed by transmission electron microscopy (TEM), X-ray diffraction, energy-dispersive X-ray spectroscopy equipped with TEM (TEM-EDX), X-ray photoelectron spectrometer, ethanol oxidation, and CO stripping. In TEM images, the $Pt_3TeRu_{0.25}$/C nanoparticles with an average particle size of around 2.9 nm were well dispersed on the carbon support. The $Pt_3TeRu_{0.25}$/C catalyst was superior to the Pt_3Te/C catalyst in respect of catalytic activity, durability, and CO tolerance. The positive effect of the Ru presence in the $Pt_3TeRu_{0.25}$/C catalyst was ascribed to the interactions of Ru or Ru oxides.

Keywords Anodic catalyst · Ethanol oxidation · Platinum · Ruthenium · Tellurium

Introduction

In the last two decades, the direct methanol fuel cell (DMFC) has drawn a great deal of attention for its simple construction and high-energy efficiency, compared with hydrogen-fed fuel cells. Much progress has been made in this field [1–4]. However, the methanol is toxic, and its crossover through the membrane also reduces the efficiency, a phenomena leading to a mixed potential observed in the oxygen reduction reaction that decreases energy efficiencies [5–8]. Therefore, researchers have looked for other small molecule alcohols as alternative fuels [9–10]. Ethanol has emerged as the first choice because it is non-toxic and can be produced in large quantities from agricultural products. Its low volatility, low price, and transportability, together with a higher-energy density than methanol (8.01 versus 6.09 kWh kg^{-1}), are also considered [11]. At the same time, the use of bioethanol will not change the natural balance of carbon dioxide in the atmosphere from the environmental viewpoint, in contrast with the use of fossil fuels [12]. So, the direct ethanol full cell (DEFC) seems promising, especially for the mobile application such as electric vehicles.

However, the complete oxidation of ethanol to CO_2 with a release of 12 electrons at temperatures compatible with available membranes is the major challenge in the electrocatalysis due to the lack of sufficiently active and selective electrocatalysts [13]. Unlike the case of DMFC, it is necessary to break the C–C bond of ethanol at low temperature. Platinum shows the highest activity for the electro-oxidation of ethanol, but the performance of pure Pt electrodes is not high due to the strongly adsorbed intermediates, which block the anode surface [14]. Therefore, a good electrocatalyst toward the complete oxidation of ethanol to CO_2 must not only avoid the poisoning of the catalytic surface by CO species as what occurs with ethanol oxidation but also activate the C–C bond breaking [15–16]. Thus, to explore novel catalysts with high anti-poisoning ability and high catalytic activity towards complete ethanol oxidation becomes a main task before ethanol could be used as a practical fuel for DEFCs. And, a lot of efforts have been reported [17]. It has been proven that the addition of other metals or metal oxides is an effective

M. Huang · L. Li · Y. Guo (✉)
College of Chemistry and Chemical Engineering,
Fuzhou University,
Fuzhou 350108, People's Republic of China
e-mail: yguo@fzu.edu.cn

way to promote the cleavage of the C–C bond and accelerate the ethanol oxidation. But, catalysts that can cleave the C–C bond of ethanol and have the ability of complete ethanol oxidation have not been obtained. At the moment, much effort was focused on the reduction of the amount of adsorbed intermediates by the addition of co-catalysts [14]. One possible way is to modify the electrode surface to increase its coverage of oxygenated species at low potentials (e.g., adsorbed OH), which are necessary to oxidize completely the intermediate species from the dissociation of ethanol to CO_2 [4]. It is well known that alkaline aqueous solutions are not stable for direct alcohol fuel cell (DAFC) due to the carbonation, and the Nafion membrane, which is very popular in DAFC, can only be used in acidic medium. So, it is better to find a new catalyst that can not only enhance the catalytic activity and CO tolerance for ethanol electro-oxidation but also be used in acidic medium [18]. At present, there are only a limited number of possible metals which are able to activate water at a low potential with sufficient stability in acid medium, including Ru, Mo, Sn, Os, W, Ir, Ni, and so on [4].

It has been found that addition of metals such as Sn and Ru to Pt catalysts can mitigate the poisoning effect of CO and enhance catalytic activity significantly [14, 19]. PtRu alloys are currently the most active anode catalyst for the oxidation of methanol or CO-contaminated H_2 (e.g., H_2 derived from reformed methanol) in solid polymer electrolyte fuel cells at low temperature, such as DMFCs [20–21] or indirect methanol fuel cells [22]. Watanabe and Motoo [23] described a bifunctional mechanism for methanol oxidation, which is related to the formation of OH on Ru atoms at low potentials, which transforms the CO adsorbed on platinum into CO_2. Other researchers [24–25] have also proposed that Ru enhances methanol oxidation through an electronic effect on neighboring Pt atoms (the ligand effect). In these mechanisms, it has been proposed that Ru may accelerate the adsorption and dehydrogenation of methanol on Pt sites at low potentials or it may weaken the Pt–CO bond, allowing the oxidation of CO at lower potentials. This decreases the polarization of methanol oxidation, which is beneficial for the practical application of low-temperature fuel cells.

In our previous works, the Pt_3Te_x/C catalysts with different atomic ratios have been synthesized, considering that the Te element is stable in acid medium. Through electrochemical characterization, we found that the Pt_3Te/C catalyst has an inferior anti-poisoning ability [26]. Based on the effects of Ru, the Ru element as the third metal is selected for achieving high anti-poisoning ability at low potentials, and the morphological structure of the synthesized ternary catalysts and their electrochemical activity for ethanol oxidation reaction have been investigated.

Experimental

$H_2PtCl_6{\cdot}6H_2O$ glycol solution (3 ml; 57.9 mM) was mixed with 20 ml glycol, 5 ml H_2O, 5.3 mg $Na_2TeO_4{\cdot}2H_2O$, $RuCl_3$ solution (Ru: 0.025 g/ml), and Vulcan XC-72 carbon in a round flask. Then, the mixture was treated in an ultrasound bath for 20 min and refluxed in an oil bath at 90 °C for 6 h in N_2 atmosphere. The excessive formic acid dissolved in glycol was added to the mixture to reduce Pt^{4+}, Te^{6+}, and Ru^{3+} completely. Finally, the mixture was washed with double-distilled water and dried at 85 °C for 8 h in a vacuum oven. The platinum nominal loading of all Pt_3TeRu_x/C catalysts with different atomic ratio is 20 wt. %, and the nominal atomic ratio of Pt/Te/Ru is 3:1:x (x=3, 1, and 0.25). Commercial PtRu/C and Pt/C are also used for comparing their catalytic activities.

The catalyst ink was prepared by mixing the catalyst in the isopropyl alcohol with a perfluorsulfonic acid solution (15 wt.% Nafion® solution) ultrasonically. A glassy carbon (GC) disk electrode with a diameter of 4 mm, which was polished to a mirror finish with a 0.05 μm gamma alumina suspension and rinsed ultrasonically with double-distilled water before each experiment, was used as the substrate for the catalyst ink. The slurry was spread on a GC disk electrode as the working electrode (area 0.1256 cm^2). Then, the electrode was dried at 80 °C, and it has 0.2 mg cm^{-2} Pt loading. A piece of Pt foil of 1.5 cm^2 was used as the counter electrode. Mercury sulfate electrode (MMS) was used as the reference one (0.62 V versus standard hydrogen electrode (SHE)). Before experiments, the 1.0 M CH_3CH_2OH+0.5 M H_2SO_4 solution or 0.5 M H_2SO_4 solution was purged with ultrapure nitrogen gas for 20 min to expel oxygen. For comparative purposes, commercial carbon-supported Pt and PtRu catalysts from Johnson Matthey Corporation (20 wt.%, molar ratio of Pt/Ru is 1:1) and the Pt_3Te/C catalyst were used.

Characterizations of the catalyst nanoparticles were carried out by Philip X'Pert Pro MPP X-ray powder diffractometer (XRD) using a Cu Kα radiation (λ= 1.5406 Å) at a scan rate of 4° min^{-1} with step of 0.01°. It was operated with a tube voltage of 40 kV, and the scan range was from 5° to 90°. The catalyst morphology and its elemental analysis were investigated by JEOL JEM-1010 transmission electron microscope (TEM) and scanning transmission electron microscopic (STEM) working at 200 kV. For microscopic examinations, the samples were first ultrasonicated in acetone for 0.5 h and then deposited on 3-mm Cu grids covered with a continuous carbon film. Electrochemical measurements were carried out in a conventional three-compartment cell. Cyclic voltammograms (CV) were obtained in a potential range of −0.6~0.6 V at a scan rate of 50 mV s^{-1} using a CHI611B electrochemical working station (CH Instrument). Due to

slight contamination, the working electrode was cycled at 50 mV s^{-1} until a stable CV response was obtained in the 0.5 M H_2SO_4 solution. The CO-stripping experiments were carried out in the following way: After recording a CV in a N_2 purged system, CO was admitted to the cell and adsorbed at 0.075 V for 30 min. The excess CO was eliminated through passing N_2 gas for 30 min, and the CV was determined by the CV between −0.6 and 0.6 V versus a MMS using a scan rate of 50 mV s^{-1}. In all experiments, analytical grades and double-distilled water were used, and the test electrolyte cell was in a water bath at 25±0.2 °C.

Results and discussion

Figure 1 shows the XRD spectra of synthesized $Pt_3TeRu_{0.25}$/C and commercial Pt/C catalysts. The diffraction peak at about 25° is corresponding to the (0 0 2) plane of the hexagonal structure of Vulcan XC-72 carbon. The characteristic diffraction peaks of Pt in the Pt/C ($Pt_3TeRu_{0.25}$/C) catalyst are clearly recognized at about 39.9° (39.3°), 46.2° (46.3°), 67.6° (67.3°), and 81.5° (80.6°) corresponding to Pt (1 1 1), (2 0 0), (2 2 0), and (3 1 1) planes, respectively. The characteristic diffraction peaks of Pt in the $Pt_3TeRu_{0.25}$/C and commercial Pt/C catalysts are characteristic of the face-centered cubic crystalline Pt (JCPDS-ICDD, Card No. 04-802). It can be seen that the peaks of $Pt_3TeRu_{0.25}$/C are shifted to the slightly lower 2θ values than that of the commercial Pt/C catalyst. No peaks of Ru and Te or their oxides were detected in the $Pt_3TeRu_{0.25}$/C catalysts, but their presence cannot be discarded because they may be present as very small crystallites, alloys, or even in an amorphous form. The Pt lattice parameter of 3.940 Å for Pt (2 2 0) peak on the $Pt_3TeRu_{0.25}$/C catalyst is larger than that of 3.918 Å on

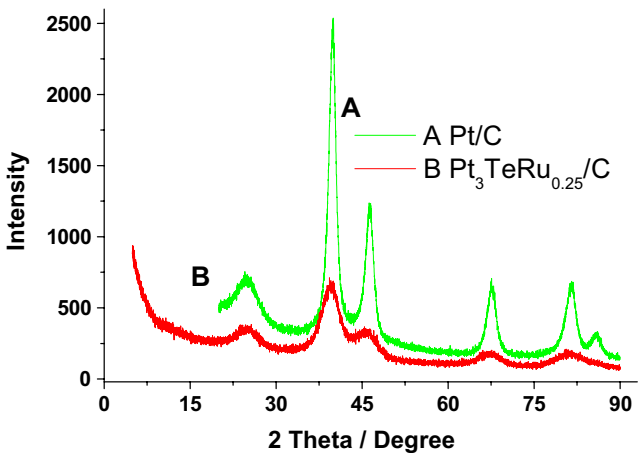

Fig. 1 XRD patterns of different catalysts: (*A*) commercial Pt/C; (*B*) synthesized $Pt_3TeRu_{0.25}$/C

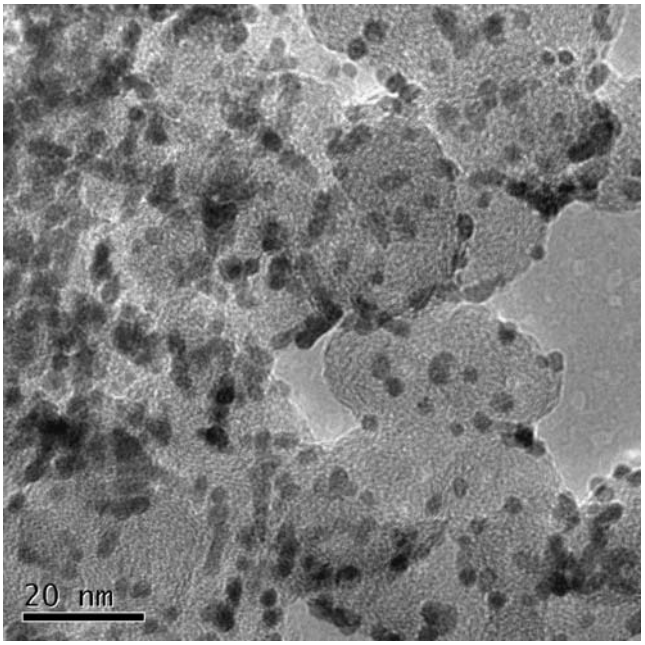

Fig. 2 TEM micrograph of the $Pt_3TeRu_{0.25}$/C catalyst

the commercial Pt/C [27]. The average particle size for the Pt_3Te/C catalyst was estimated from the XRD peak of the (2 2 0) plane by using Sherrer's formula and was 2.2 nm [28].

Figure 2 shows TEM image of the $Pt_3TeRu_{0.25}$/C catalyst. In TEM image, most of $Pt_3TeRu_{0.25}$/C particles are uniform and highly dispersed on the surface of carbon black. The good distribution of the $Pt_3TeRu_{0.25}$/C nanoparticles is known to be important for the catalytic activity [29]. It should be noted that Pt, Te, and Ru or their oxides particles cannot be distinguished because of the similar darkness in TEM image. It is found that there is no diffraction peak of Te and Ru or their oxides in the XRD patterns of $Pt_3TeRu_{0.25}$/C, which means that they are amorphous or they are very small crystallites. This can be confirmed from energy-dispersive X-ray (EDX) analyses. The size distribution of $Pt_3TeRu_{0.25}$ nanoparticles on the carbon support was obtained by measuring the sizes of 197 particles chosen randomly from TEM images. Figure 3 depicts a sharp distribution of its metal particle size, and its mean particle size is about 2.9 nm. The mean particle size is in good agreement with the XRD result. The state of Te and Ru in $Pt_3TeRu_{0.25}$/C catalyst was then analyzed. In Fig. 4, TEM-EDX analysis was carried out in the center of the catalyst particle and on the surface of carbon support, where there was no catalyst particle. The analyzed points are shown as red circles (1 and 2) in TEM image. Pt, Te, and Ru were not detected on the surface of carbon support (analyzed point 2). On the contrary, Pt, Te, and Ru are detected on the catalyst particles (analyzed point 1). The fact indicates that Pt^{4+}, Te^{6+}, and Ru^{3+} were reduced and

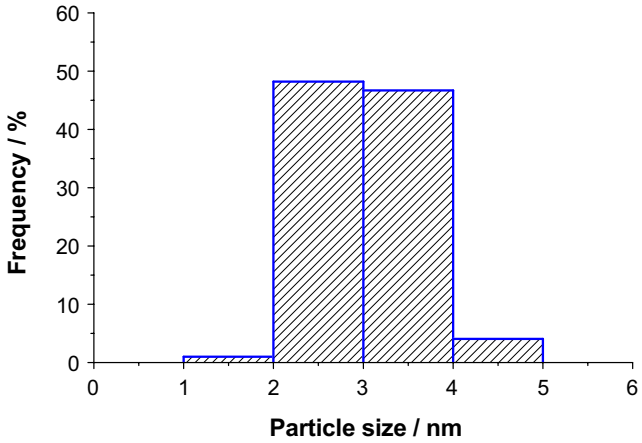

Fig. 3 The Pt_3Te/C particle size distribution

coexisted together, which plays a significant role in improving catalytic activity of the $Pt_3TeRu_{0.25}/C$ catalyst.

In order to know the electrochemical behavior of the synthesized catalyst, the mass activity (MA; amper per gram), defined by peak current density (milliamper per square centimeter, i_p) per Pt loading mass (milligrams per square centimeter, M), is used to evaluate the electrochemical activity of catalyst for ethanol oxidation in this paper, i.e., $MA=i_p/M$. Because the mass-normalized current density represents the economic efficiency of the catalysts, it is generally adopted instead of the area-normalized one in similar catalytic environments resulting in the same qualitative trends. Figure 5 shows the cyclic voltammograms of ethanol oxidation on synthesized catalysts with different atomic ratios. Obviously, the addition of Ru makes the peak potential shift in the negative direction in the forward and backward scans. It is clear from Fig. 5 that although the shifted peak potentials of the ternary Pt–Te–Ru catalysts depend on the Ru content, their peak current density decreases with the increase of Ru content. It is possible that the Pt sites are covered when more Ru is added. So, the content of Ru needs a suitable ratio for lowing peak potential and increasing peak current density. The $Pt_3TeRu_{0.25}/C$ catalyst has higher anodic peak current and lower peak potential of ethanol oxidation than the Pt_3Te/C catalyst. The forward scan peak potentials on $Pt_3TeRu_{0.25}/C$, Pt_3TeRu/C, Pt_3TeRu_3/C Pt_3Te/C, and commercial PtRu/C are 260, 240, 240, ,287 and 270 mV (versus MMS), respectively. Their corresponding peak current densities are 1,065, 752, 575, 1,002, and 817.6 A g^{-1}. A low I_f/I_b ratio (I_f is designated as forward current density, and I_b is designated as backward current density) indicates poor oxidation of ethanol to carbon dioxide during the anodic scan and excessive accumulation of carbonaceous residues on the catalyst surface. A high I_f/I_b ratio shows the converse case [30–31]. In Fig. 5, the ratio of the forward to reverse anodic peak current density, I_f/I_b, is used to describe the tolerance of the catalyst to the accumulation of carbonaceous species. From the results in Fig. 5, their ratios are 1.57, 1.65, 1.36, 1.44, and 1.55 for $Pt_3TeRu_{0.25}/C$,

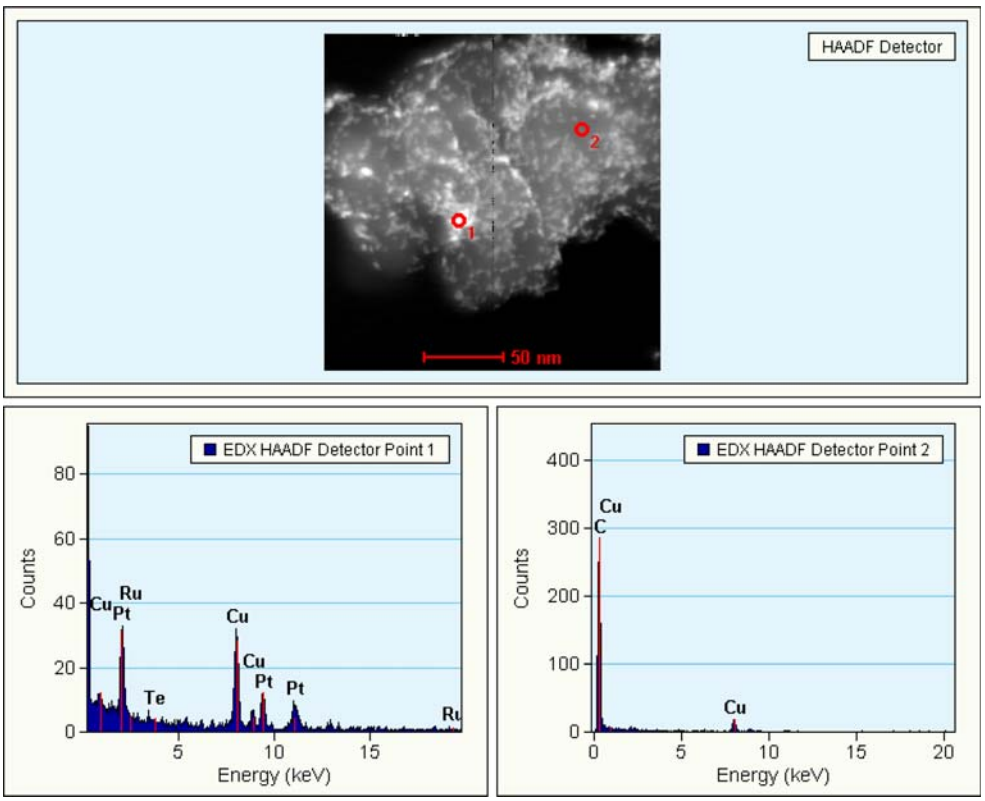

Fig. 4 STEM spectrum of the $Pt_3TeRu_{0.25}/C$ catalyst in TEM-EDX analysis. *Red circles* show the analyzed points by TEM-EDX and the strong Cu-peak originates from the Cu supporting grid

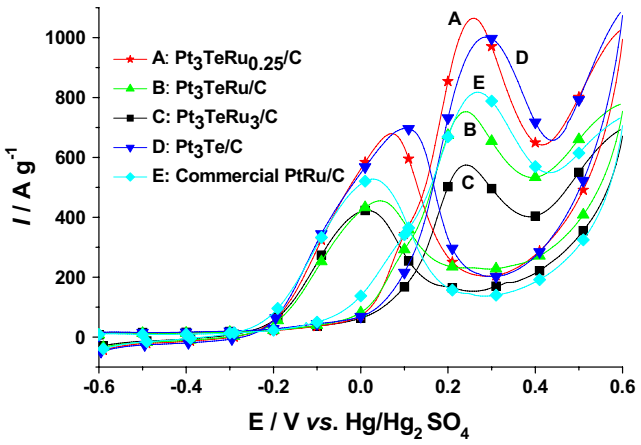

Fig. 5 The cyclic voltammograms of ethanol oxidation on different catalysts at 50 mV s^{-1} in 1 M C_2H_5OH+0.5 M H_2SO_4

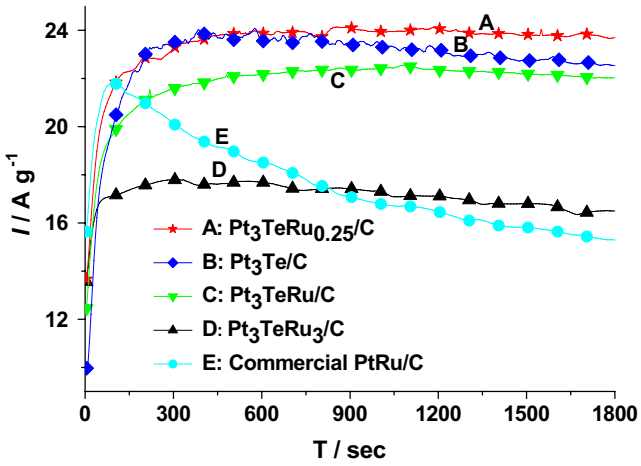

Fig. 6 Current-time curves on different catalysts at 0.82 V (versus SHE) in 1 M C_2H_5OH+0.5 M H_2SO_4

Pt_3TeRu/C, Pt_3TeRu_3/C, Pt_3Te/C, and commercial PtRu/C, respectively. So, the anti-poisoning ability has the following order: Pt_3TeRu/C > $Pt_3TeRu_{0.25}/C$ > commercial PtRu/C > Pt_3Te/C> Pt_3TeRu_3/C. Therefore, the anti-poisoning ability of $Pt_3TeRu_{0.25}/C$ catalyst is improved by addition of Ru, but still lower than the catalysts with high Ru content, such as Pt_3TeRu/C.

The average size of $Pt_3TeRu_{0.25}/C$ catalyst obtained from XRD peak and TEM image is 2.2 and 2.9 nm, respectively, and it is 2.4 and 2.8 nm for Pt_3Te/C catalyst. This implies that the specific surface area of the $Pt_3TeRu_{0.25}/C$ nanocatalyst is approximately the same as that of the Pt_3Te/C. Compared to the Pt_3Te/C catalyst, the synthesized $Pt_3TeRu_{0.25}/C$ catalyst has the lower peak potential and the higher anodic peak current density. So, the addition of Ru enhances the electrochemical activity of the Pt_3Te/C nanocatalyst for ethanol electro-oxidation. The superior activity of the $Pt_3TeRu_{0.25}/C$ electrocatalyst may be attributed to the electronic modification of Pt and the presence of Ru and its oxide species, which may play the role of electronic effect and bifunctional mechanism[32–34].

The performance of Pt_3TeRu_x/C and Pt_3Te/C eletrocatalysts for ethanol oxidation was also studied by chronoamperometry (CA) in 1 M C_2H_5OH+0.5 M H_2SO_4 solution at 0.5 and 0.82 V versus SHE, and their current-time curves are shown in Figs. 6 and 7, respectively. The current values were normalized per gram of platinum, considering that ethanol adsorption and dehydrogenation occur only on platinum sites at room temperature. Figure 6 shows that the current increases quickly and then drops slowly. It is found that the current obtained for $Pt_3TeRu_{0.25}/C$ electrocatalyst is the highest and quite steady. The order of the activity for ethanol electro-oxidation is $Pt_3TeRu_{0.25}/C$ > Pt_3Te/C > Pt_3TeRu/C > Pt_3TeRu_3/C > commercial PtRu/C. It is worth mentioning that Ru makes the current on $Pt_3TeRu_{0.25}/C$ more steady at low potential, compared with Pt_3Te/C. The improved anti-poisoning ability of the $Pt_3TeRu_{0.25}/C$ catalyst may be explained by the electronic modification of platinum and bifunctional mechanism, in which the reaction between weakly bound Pt_3CO species and OH_{ads} on neighboring Ru and Te sites constitutes the main mechanism of intermediate species removal [32–34]. Figure 7 shows that the current begins to drop quickly, then decrease slowly. It is found that the current values obtained for $Pt_3TeRu_{0.25}/C$ eletrocatalyst is the highest. The order of durability for ethanol electro-oxidation is $Pt_3TeRu_{0.25}/C$ ≈ commercial PtRu/C > Pt_3TeRu/C > Pt_3TeRu_3/C ≈ Pt_3Te/C. When the electrode is polarized at 0.5 V due to the continuous oxidation of ethanol on the catalyst surface, reaction intermediates such as CO_{ads} would begin to accumulate if the kinetics of the removal reaction could not keep pace with that of ethanol oxidation. A slower decay of current density with time implies that the catalyst has good anti-poisoning ability.

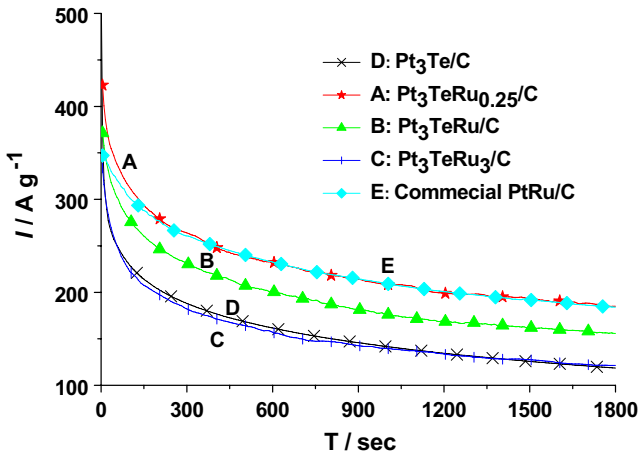

Fig. 7 Current-time curves on different catalysts in 1 M C_2H_5OH+0.5 M H_2SO_4 at 0.50 V (versus SHE)

The activity of the $Pt_3TeRu_{0.25}$/C and Pt_3Te/C catalysts for CO oxidation was investigated by CO-stripping voltammetry at 50 mV s^{-1}, during which CO was adsorbed on the catalysts at −0.615 (versus MMS) for 30 min. Commercial PtRu/C and Pt/C are also used for comparing their CO tolerance. The CO-stripping voltammograms of the $Pt_3TeRu_{0.25}$/C, Pt_3Te/C, and commercial PtRu/C and Pt/C catalysts are shown in Fig. 8. The order of onset potential of CO oxidation is commercial PtRu/C > $Pt_3TeRu_{0.25}$/C > Pt_3Te/C > commercial Pt/C. This indicates that the activity of the commercial PtRu/C catalyst for CO oxidation is superior to other catalysts. It appears that Ru has the ability to promote the oxidation of adsorbed CO at low potentials. The shift of the onset potential on the $Pt_3TeRu_{0.25}$/C catalyst may be attributed to the presence of oxygenated species on the Ru sites at lower potential and the electronic effect as compared to Pt_3Te/C and Pt/C catalysts [17, 32–34]. The shift of the onset potential to a lower value in the CO-stripping voltammograms for the $Pt_3TeRu_{0.25}$/C catalyst is in agreement with the findings of CA and CV as compared to Pt_3Te/C. Moreover, the range of potentials allowing for the oxidation of CO on the $Pt_3TeRu_{0.25}$/C catalyst is wider than that on the Pt_3Te/C catalyst. So, the addition of a little Ru enhances the CO tolerance of Pt_3Te catalyst greatly.

The state or role of Ru has been investigated and is quite clear. In order to understand the activity of the Pt_3Te/C electrocatalyst, surface composition characterization was carried out by employing X-ray photoelectron spectrometer (XPS). The core level spectra of Pt 4f and Te 3d for Pt_3Te/C electrocatalyst are shown in Figs. 9 and 10, respectively. The two most intense peaks in Fig. 9, located at the binding energies of 71.25 eV (for Pt $4f_{7/2}$) and 74.6 eV (for Pt $4f_{5/2}$), maintain an area ratio near 4:3 as expected theoretically for pure Pt (71.20 eV of Pt $4f_{7/2}$ and 74.53 eV of Pt $4f_{5/2}$), and their positions shift higher [33]. Hence, it is obvious

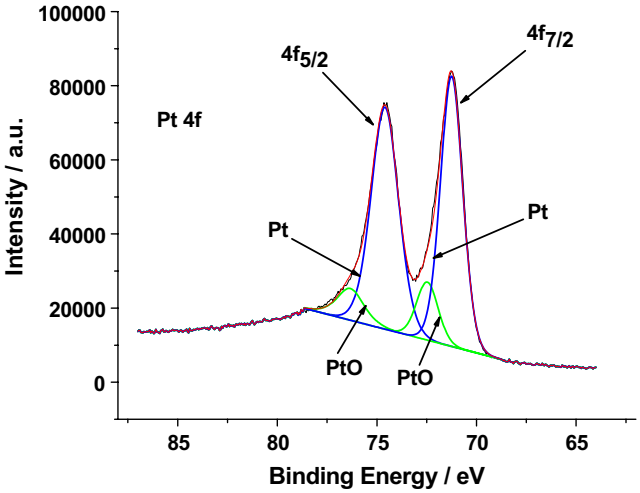

Fig. 9 XPS core level spectra for the Pt 4f photoemission from the Pt_3Te/C nanoparticles

that they originate from metallic Pt^0. The peaks at 72.5 and 76.4 eV can be attributed to Pt^{2+} in the form of PtO, which can be electrochemically reduced [35]. The result of deconvolution indicates a phase composition, which contains 80.0% of Pt in metallic Pt^0 and 20% in Pt^{2+} (as PtO). In spite of the low intensity and therefore the relatively high background noise contribution in the Te 3d core level region, the Te 3d spectrum was deconvoluted into four peaks. The two most intense peaks in Fig. 10 are at the binding energies of 573.45 eV (for Te $3d_{5/2}$) and 583.9 eV (for Te $3d_{3/2}$), and they are attributed to Te^0. The peaks at 575.75 and 586.4 eV can be attributed to TeO_2. The result of deconvolution indicates a phase composition, which contains 65.4% of Te^0 and 34.6% TeO_2. The calculation shows that the large fraction of Pt (about 80%) and Te (about 65.4%) is in the state Pt^0 and Te^0, while a much smaller fraction exists as PtO (about 17.5) and TeO_2 (about 34.6%). These bands of Pt undergo a shift to higher energy

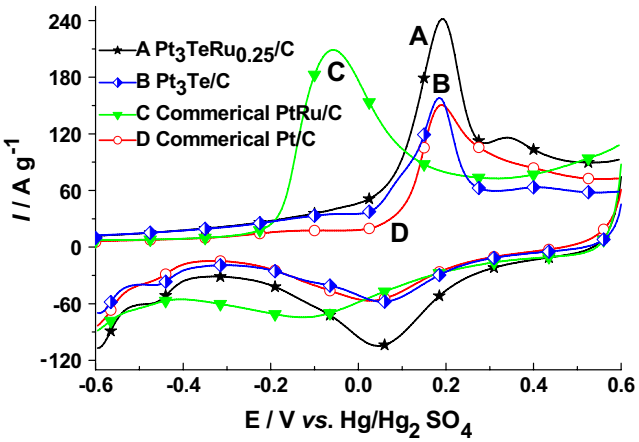

Fig. 8 CO-stripping voltammograms on different catalysts at 50 mV s^{-1} in 0.5 M H_2SO_4 solutions

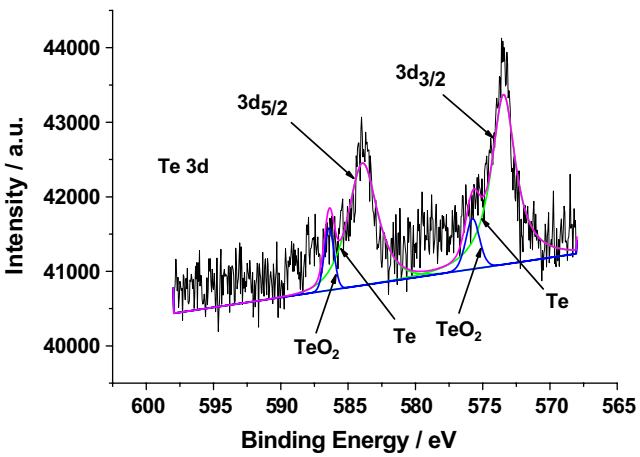

Fig. 10 XPS core level spectra for the Te 3d photoemission from the Pt_3Te/C nanoparticles

and that is due to a charge transfer process from Pt to Te [36]. In the meantime, the Pt_3Te/C nanocatalyst has an enhanced activity than synthesized Pt/C catalysts [26], but its anti-poisoning ability is lower. So, the role of Te on Pt_3Te/C nanocatalysts may be the electronic modification of platinum, which may play the role of electronic effect [3, 32–34, 37].

Conclusions

Ru as the third element was selected for ethanol electro-oxidation in sulfuric acid solution, and the Pt_3TeRu_x/C nanocatalysts were successfully prepared, and well-dispersed nanoparticles with a sharp distribution were obtained with its mean particle size of about 2.9 nm. The EDX analysis shows that Pt^{4+}, Te^{6+}, and Ru^{3+} were reduced and coexisted together, which plays a significant role in improving catalytic activity of the $Pt_3TeRu_{0.25}/C$ catalyst. The $Pt_3TeRu_{0.25}/C$ is superior to other similarly synthesized Pt_3TeRu_x/C and Pt_3Te catalysts, in aspects of the catalytic activity, the CO tolerance, and the durability in the acidic solution. Regarding the oxidation of adsorbed CO, the $Pt_3TeRu_{0.25}/C$ catalyst exhibited a lower onset potential than the Pt_3Te/C catalyst, revealing that the contribution of oxidative removal of the intermediate C1 and C2 species from the Pt sites is mainly due to the Ru. The effect of Ru in the $Pt_3TeRu_{0.25}/C$ nanoparticles may be explained through the bifunctional mechanism and the modification of the Pt electronic states. The XPS results show that the role of Te on Pt_3Te/C nanocatalysts may be the electronic modification of platinum, which may play the role of electronic effect. But, a novel catalyst with high anti-poisoning ability and high catalytic activity towards complete ethanol oxidation is still an arduous task, and the breakthrough is necessary for a practical application of DEFCs.

References

1. Uchida H, Mizuno Y, Watanabe M (2002) J Electrochem Soc 149: A682. doi:10.1149/1.1471539
2. Choi WC, Kim JD, Woo SI (2002) Catal Today 74:235. doi:10.1016/S0920-5861(02)00026-3
3. Wang ZB, Yin GP, Shi PF (2006) Carbon 44:133. doi:10.1016/j.carbon.2005.06.043
4. Wang ZB, Yin GP, Lin YG (2007) J Power Sources 170:242. doi:10.1016/j.jpowsour.2007.03.078
5. Spinacé EV, Neto AO, Linardi M (2004) J Power Sources 129:121. doi:10.1016/j.jpowsour.2003.11.056
6. Pinheiro ALN, Neto AO, Souza EC, Ticianelli EA, Perez J, Gonzalez ER (2003) J. N Mater Electrochem. Syst 6:1
7. Iwasita T (2002) Electrochim Acta 47:3663. doi:10.1016/S0013-4686(02)00336-5
8. Liu ZL, Hong L, Tay SW (2007) Mater Chem Phys 105:222. doi:10.1016/j.matchemphys.2007.04.045
9. Lamy C, Belgsir EM, Leger JM (2001) J Appl Electrochem 31:799. doi:10.1023/A:1017587310150
10. Spinacé EV, Neto AO, Linardi M (2003) J Power Sources 124:426. doi:10.1016/S0378-7753(03)00808-5
11. Zhou WJ, Song SQ, Li WZ, Zhou ZH, Sun GQ, Xin Q, Douvartzides S, Tsiakaras P (2005) J Power Sources 140:50. doi:10.1016/j.jpowsour.2004.08.003
12. Vigier F, Coutanceau C, Hahn F, Belgsir EM, Lamy C (2004) J Electroanal Chem 563:81. doi:10.1016/j.jelechem.2003.08.019
13. Song SQ, Tsiakaras P (2006) Appl. Catal. B Environ. 63:187. doi:10.1016/j.apcatb.2005.09.018
14. Suffredini HB, Banda GRS, Avaca LA (2007) J Power Sources 171:355. doi:10.1016/j.jpowsour.2007.06.048
15. Leger JM, Rousseau S, Coutanceau C, Hahn F, Lamy C (2005) Electrochim Acta 50:5118. doi:10.1016/j.electacta.2005.01.051
16. Wang H, Jusys Z, Behm RJ (2004) J Phys Chem B 108:19413. doi:10.1021/jp046561k
17. Wu G, Swaidan R, Cui GF (2007) J Power Sources 172:180. doi:10.1016/j.jpowsour.2007.07.034
18. Song HQ, Qiu XP, Li FS, Zhu WT, Chen LQ (2007) Electrochem Commun 9:1416. doi:10.1016/j.elecom.2007.01.048
19. Simões FC, dos Anjos DM, Vigier F, Léger JM, Hahn F, Coutanceau C, Gonzalez ER, Tremiliosi-Filho G, de Andrade AR, Olivi P, Kokoh KB (2007) J Power Sources 167:1. doi:10.1016/j.jpowsour.2006.12.113
20. Ren X, Wilson MS, Gottesfeld S (1996) J Electrochem Soc 143: L12. doi:10.1149/1.1836375
21. Wasmus S, Vielstich W (1993) J Appl Electrochem 23:120. doi:10.1007/BF00246948
22. Oetjen HF, Schmidt VM, Stimming U, Trila F (1996) J Electrochem Soc 143:3838. doi:10.1149/1.1837305
23. Watanabe M, Motoo S (1975) J Electroanal Chem 60:267. doi:10.1016/S0022-0728(75)80261-0
24. Krausa M, Vielstich W (1994) J Electroanal Chem 379:307. doi:10.1016/0022-0728(94)87152-3
25. Tong YY, Kim HS, Babu PK, Waszczuk P, Wieckowski A, Oldfield E (2002) J Am Chem Soc 124:468. doi:10.1021/ja011729q
26. Huang MH, Wang F, Li LR, Guo YL (2008) J Power Sources 178:48. doi:10.1016/j.jpowsour.2007.12.056
27. Jiang LH, Zhou ZH, Li WH, Zhou WJ, Song SQ, Li HQ, Sun GQ, Xin Q (2004) Energy Fuels 18:866. doi:10.1021/ef034073q
28. Roychowdhury C, Matsumoto F, Zeldovich VB, Warren SC, Mutolo PF, Ballesteros M, Wiesner U, Abruna HD, Disalvo FJ (2006) Chem Mater 18:3365. doi:10.1021/cm060480e
29. Lee DY, Hwang SW, Lee IS (2005) J Power Sources 145:147. doi:10.1016/j.jpowsour.2005.02.067
30. Liu ZL, Ling XY, Su XL, Lee JY, Gan LM (2005) J Power Sources 149:1. doi:10.1016/j.jpowsour.2005.02.009
31. Liu ZL, Hong L (2007) J Appl Electrochem 37:505. doi:10.1007/s10800-006-9282-0
32. Spinacé EV, Linardi M, Neto AO (2005) Electrochem Commun 7:365. doi:10.1016/j.elecom.2005.02.006
33. Choi JH, Park KW, Kwon BK, Sung YE (2003) J Electrochem Soc 150:A973. doi:10.1149/1.1581011
34. Park KW, Choi JH, Lee SA, Pak C, Chang H, Sung YE (2004) J Catal 224:236. doi:10.1016/j.jcat.2004.02.010
35. Bock C, Paquet C, Couillard M, Botton GA, MacDougall BR (2004) J Am Chem Soc 126:8028. doi:10.1021/ja0495819
36. Park KW, Choi JH, Kwon BK, Lee SA, Sung YE, Ha HY, Hong SA, Kim H, Wieckoswski A (2002) J Phys Chem B 106:1869. doi:10.1021/jp013168v
37. Moreno B, Chinarro E, Fierro JLG, Jurado JR (2007) J Power Sources 169:98. doi:10.1016/j.jpowsour.2007.01.051